PROCEEDINGS OF THE ROYAL SOCIETY A MATHEMATICAL, PHYSICAL & ENGINEERING SCIENCES

Effects of reduced dimensionality on the electronic structure and defect chemistry of semiconducting hybrid organic–inorganic PbS solids

Aron Walsh

Proc. R. Soc. A 2011 **467**, 1970-1985 first published online 9 February 2011
doi: 10.1098/rspa.2010.0514

PROCEEDINGS OF THE ROYAL SOCIETY A

Proc. R. Soc. A (2011) **467**, 1970–1985
doi:10.1098/rspa.2010.0514
Published online 9 February 2011

Effects of reduced dimensionality on the electronic structure and defect chemistry of semiconducting hybrid organic–inorganic PbS solids

By Aron Walsh*

Kathleen Lonsdale Materials Chemistry, Department of Chemistry, University College London, 20 Gordon Street, London WC1H 0AJ, UK

The combination of inorganic and organic frameworks to produce crystalline hybrid semiconductors offers a pathway for obtaining novel photovoltaic and optoelectronic materials. Taking an archetypal binary semiconductor, PbS (galena), we investigate the electronic effects of the reduced dimensionality in the PbS framework on transition from bulk PbS to three-dimensional and one-dimensional hybrid inorganic–organic networks. Analysis of density functional theory calculations reveals the substantial contribution of the organic (benzenehexathiol derivates) to the band-edge states. Implications for intrinsic defect formation and potential application in solar cell devices are discussed, as well as future design pathways for engineering the electronic properties of this new class of hybrid metal–organic framework.

Keywords: metal sulphides; defects; hybrid materials; density functional theory

1. Introduction

Traditionally, there has been a clear separation between the materials chemistry of organic and inorganic systems; however, the discovery of organic–inorganic hybrid frameworks has resulted in an emerging theme at the interface of these two disciplines (Ferey 2001; Cheetham & Rao 2007). The resulting inorganic–organic hybrid materials are crystalline and can be reproducibly fabricated. This rapidly growing family of compounds can be classified based on the dimensionality of the inorganic (I) and organic (O) linkages: I_xO_y, where $x + y \leq 3$ (Cheetham *et al.* 2006; Rao *et al.* 2008). To date, the majority of research has centred on metal organic frameworks (MOFs) with I_0O_y ($y = 1$–3). This special class of coordination polymers contains isolated metal cations linked through functional organic moieties and offers potential for gas storage and catalysis, and are generally viewed as the hybrid analogues of classical porous zeolites (Mellot-Draznieks 2007). For electronic applications however, MOFs often offer

*a.walsh@ucl.ac.uk

One contribution of 16 to a Special feature 'High-performance computing in the chemistry and physics of materials'.

Received 7 October 2010
Accepted 19 November 2010

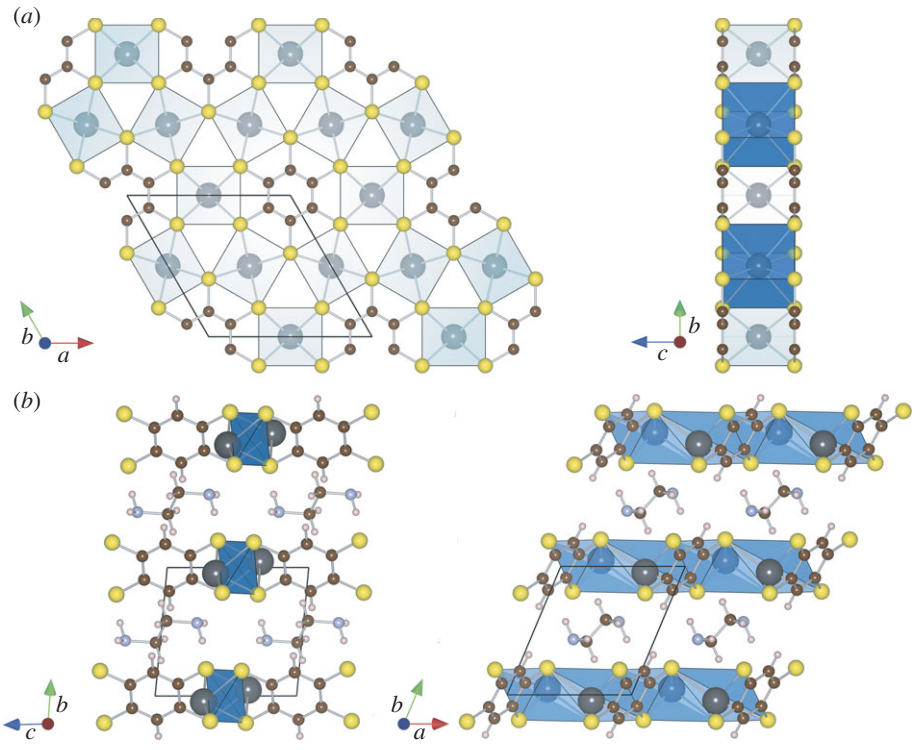

Figure 1. Crystal structure representations of (*a*) $Pb_3(C_6S_6)$ and (*b*) $Pb_2(S_4C_6H_2)(en)$ containing three-dimensional and one-dimensional hybrid PbS networks, respectively. The carbon atoms are coloured brown, with grey Pb, yellow S and pink hydrogen. (Online version in colour.)

mediocre structural stability, wide band gaps and feature poor semiconducting properties, with the exception of the ZnO-based MOF-5 and related compounds (Alvaro *et al.* 2007).

In contrast to MOFs, hybrid systems containing higher dimensionality in the inorganic networks, introducing the possibility of novel anisotropic electronic, magnetic and optical effects, with improved thermal and chemical stability, have been relatively neglected; two notable exceptions being experimental work from the groups of Li (Zhang *et al.* 2006; Guo *et al.* 2009; Huang *et al.* 2009) and Maggard (Lin & Maggard 2007, 2008; Lin *et al.* 2009). Furthermore, there has been no systematic approach established for achieving or improving desirable material properties. Here, we take an archetypal binary inorganic semiconductor with excellent electron transport properties, PbS, and investigate the changes in the electronic structure on the formation of hybrid organic–inorganic PbS networks. Hybrid compounds of PbS have demonstrated a remarkable versatility in their inorganic dimensionality, with crystal structures reported for PbS networks ranging from one dimension to three dimensions, as illustrated in figure 1. For example, $Pb_3(C_6S_6)$ contains three-dimensional networks of edge-sharing PbS cubes, while $Pb_2(S_4C_6H_2)(en)$, where *en* represents the ethylenediamine ligand, contains one-dimensional kinked chains of PbS

stacked along the triclinic *a*-axis. These two materials exhibit optical band gaps of 1.7 and 3.1 eV, respectively (Turner *et al.* 2008), covering the full range of the visible spectrum. This demonstrates the potential of hybrid materials for optoelectronic applications including photovoltaics and solid-state lighting, areas traditionally dominated by III–V, II–VI and related semiconductor alloys (Srivastava *et al.* 1985; Wei *et al.* 1990; Zhu *et al.* 2008; Chen *et al.* 2009*b*; Catlow *et al.* 2010).

In this work, we investigate changes in the electronic structure produced from the parent rocksalt-structured PbS on the formation of hybrid materials containing PbS polyhedra linked through three-dimensional and one-dimensional networks with benzenehexathiol-derived organic ligands. Our calculations, based on a first-principles density functional theory approach, highlight the effect of quantum confinement in widening the intrinsic PbS band gap, in addition to the marked contributions of the organic components to the band-edge states and also to point defect formation. Finally, a design rationale for further engineering the electronic properties of hybrid materials is proposed.

2. Computational methods

The electronic structure and total energy of rocksalt PbS and both hybrid PbS systems were calculated using density functional theory (DFT; Hohenberg & Kohn 1964; Kohn & Sham 1965) within the code VASP (Kresse & Furthmüller 1996*a*,*b*). Exchange-correlation effects were treated at the generalized gradient approximation (GGA) level of theory, namely the Perdew–Burke Ernzerhof (PBE) functional (Perdew *et al.* 1996). A plane-wave basis set was employed, with the projector augmented wave method (Blöchl 1994) used to represent the valence–core (Pb:[Xe], C:[He], N:[He], S:[Ne]) interactions. Scalar-relativistic contributions are explicitly included in the core potentials, while spin–orbit coupling is not treated; previous calculations on PbS have shown that the inclusion of spin–orbit coupling lowers the degeneracy of the empty Pb 6*p* band, but does not significantly affect the valence band structure (Wei & Zunger 1997). All calculations were performed on the HECToR supercomputer using, on average, 128 cores for a typical optimization job. The parallel efficiency of VASP (and similar plane-wave DFT codes) dramatically decreases for larger numbers of cores, primarily due to the increased cost (latency) of communication between the computing nodes.

The plane-wave kinetic energy cut-off (500 eV) and the *k*-point sampling were both checked for convergence in both the total energies and equilibrium lattice constants. The internal positions were relaxed using Quasi-Newton minimization until the forces were below $0.005\,\mathrm{eV\,\AA^{-1}}$. The equilibrium cell volumes were obtained by performing a series of constant volume calculations and fitting the resulting energy–volume data to the Murnaghan equation of state (Murnaghan 1944). The electronic band structures are plotted along high symmetry directions of the respective first Brillouin zone of the primitive unit cells (Aroyo *et al.* 2006), which are illustrated for the two hybrid material structures in figure 2. The lattice site and angular momentum decomposed (local) electronic densities of states were obtained by projecting the wavefunctions onto spherical harmonics centred at each ion core.

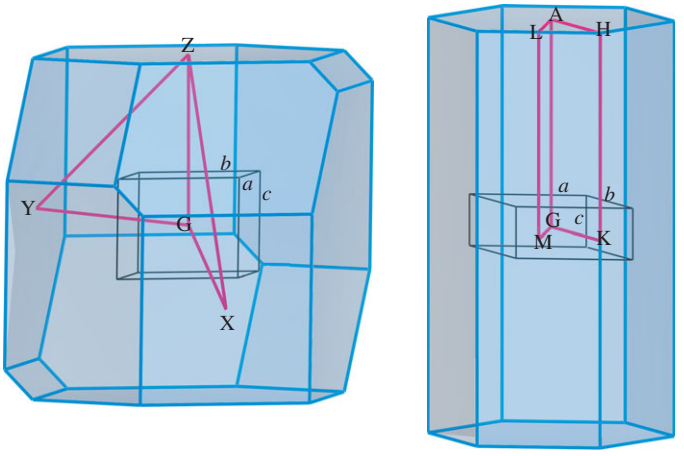

Figure 2. Representations of the 1st Brillouin zones (shaded polyhedron) for the one-dimensional (left) and three-dimensional (right) hybrid PbS structures, and the high symmetry lines sampled in this study (thick dark grey line). The corresponding triclinic and hexagonal unit cells are drawn with thin black lines, with lattice vectors a, b and c. (Online version in colour.)

To provide a more accurate assessment of the electronic band gaps of the materials of interest, further calculations were performed using a hybrid density functional that replaces 25 per cent of the semi-local PBE exchange potential with non-local Hartree–Fock exact exchange (Dovesi *et al.* 1981). The exchange potential is partitioned into short-range (SR) and long-range (LR) contributions, using a screening parameter of $\omega = 0.11\,\mathrm{Bohr}^{-1}$, resulting in the HSE06 functional (Heyd & Scuseria 2004; Hummer *et al.* 2009), as implemented in version 5 of the code VASP (Paier *et al.* 2006; Marsman *et al.* 2008):

$$E_{xc}^{\mathrm{HSE06}} = E_{c}^{\mathrm{PBE}} + \left[\tfrac{3}{4}E_{x}^{\mathrm{PBE}} + \tfrac{1}{4}E_{x}^{\mathrm{HF}}\right]^{\mathrm{SR}(\omega)} + \left[E_{x}^{\mathrm{PBE}}\right]^{\mathrm{LR}(\omega)}. \tag{2.1}$$

While there is an established system and property dependence of the amount of exchange required to yield accurate observables (Corà *et al.* 2004; Walsh *et al.* 2008), the HSE06 functional has demonstrated recent success and transferability in describing the structural, electronic and defect properties of semiconducting and insulating systems (Brothers *et al.* 2008; Hummer *et al.* 2009; Scanlon *et al.* 2009; Chen *et al.* 2009*a*; Walsh *et al.* 2009*b*).

3. Results

(*a*) *Galena*

Lead sulphide is found naturally as the mineral galena, and is one of the most abundant metal sulphide compounds. The surface oxidation process is of significant environmental interest and has been the subject of previous theoretical investigation (Wright *et al.* 1999*a*,*b*). In relation to technological applications, PbS is a narrow band gap semiconductor that has attracted significant attention for quantum dot and multiple-exciton-generation solar cells

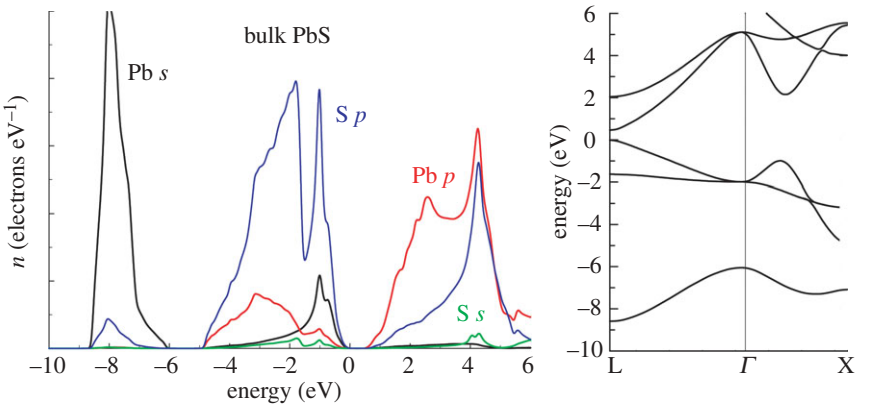

Figure 3. The local electronic density of states and band structure of rocksalt PbS at the GGA level of theory. The highest occupied state is set to 0 eV. (Online version in colour.)

(Nozik 2005). In quantum-confined PbS systems, it has been demonstrated that a single photon of light (much higher in energy than the material band gap) can generate multiple electron–hole pairs, in what can be viewed as an inverse Auger process (Ellingson *et al.* 2005). Despite initial excitement over high internal quantum yields (more than 300%), with the prospect of achieving light-to-electricity conversion efficiencies beyond the single-junction Shockley & Queisser (1961) limit in these 'third-generation' photovoltaic cells, difficulties arise in the extraction of the photo-generated electron–hole pairs *before* recombination, and thus far improved device efficiencies based on multiple-excition generation have not been reported to our knowledge. The formation of hybrid material systems may provide an opportunity to overcome these limitations in the future.

In contrast to PbO, which exhibits asymmetric Pb coordination and a low symmetry layered structure, PbS adopts a centrosymmetric rocksalt lattice with $a = 5.936$ Å (Madelung 2004); these structural preferences have been related to the energy separation between the Pb 6*s* and anion n*p* orbitals (Walsh & Watson 2005; Payne *et al.* 2006), with similar effects observed for other lone pair ceramics including those of Sn(II) and Bi(III) (Walsh & Watson 2004; Walsh *et al.* 2009*c*; Catlow *et al.* 2010). In its bulk form, PbS has a room temperature direct band gap of 0.420 eV at the L point of the first Brillouin zone (Madelung 2004). This small electronic gap results in remarkably low hole and electron effective masses of 0.08 m_e and corresponding Hall mobility greater than 10 000 $\mathrm{cm^2\ V\ s^{-1}}$ at low temperatures (Zemel *et al.* 1965). The heavier lead monochalcogenides exhibit similar structural preferences, with rocksalt structured PbSe ($a = 6.124$ Å, $E_g = 0.28$ eV) and PbTe ($a = 6.462$ Å, $E_g = 0.31$ eV) (Madelung 2004).

The equilibrium GGA lattice constant of PbS is 6.006 Å, within 1.5 per cent of experimental data. The calculated electronic density of states (DOS) and band structure are shown in figure 3. The occupied Pb 6*s* band is present between −6 and −8 eV, with evidence of some hybridization with S 3*p*. The three predominately S 3*p* bands are located between −5 and 0 eV; these bands are degenerate at the gamma point, but split towards the L $2\pi/a(1/2, 1/2, 1/2)$ and X $2\pi/a(1/2, 0, 1/2)$ special points. The GGA fundamental band gap is direct

Table 1. The equilibrium GGA structural and electronic parameters of the bulk and hybrid PbS systems. The band gaps obtained from the hybrid HSE06 functional are also listed for comparison. The corresponding experimental values (Madelung 2004; Turner *et al.* 2008) are shown in parenthesis. Note that the experimental band gaps were estimated from room temperature visible light absorption spectra for the hybrid materials.

	bulk PbS	three-dimensional hybrid	one-dimensional hybrid
a (Å)	6.006 (5.936)	9.053 (8.964)	7.192 (6.938)
b (Å)			7.356 (7.145)
c (Å)		4.006 (3.958)	8.078 (7.891)
α (°)	90	90	85.60 (85.89)
β (°)	90	90	65.98 (66.56)
γ (°)	90	120	68.07 (67.59)
Pb–S (Å)	6 × 3.00	8 × 3.11	6 × 3.22
E_g^{GGA}(eV)	0.47 (0.42)	0.99 (1.7)	2.22 (3.1)
E_g^{HSE06}(eV)	0.84 (0.42)	1.84 (1.7)	3.15 (3.1)

at the L point (0.465 eV), with the conduction band composed predominately of Pb 6p states. The occurrence of the direct band gap away from the gamma point has been explained by the hybridization between Pb 6s and S 3p, which is symmetry forbidden (Wei & Zunger 1997), i.e. in the rocksalt primitive unit cell, interatomic σ bonding between s and p states are forbidden at the zone centre due to their phase inequivalence (A_{1g} and T_{2u} representations, respectively). Similar restrictions for the coupling of p and d states results in the indirect band gap of CdO (Mcguinness *et al.* 2003; Zhu *et al.* 2008). In comparison to experiment, the magnitude of the band gap for PbS is in good agreement; while this level of theory typically underestimates the band gaps of insulating materials, for the case of band gaps determined by anion and cation p orbitals, better agreement is generally found (Wei & Zunger 1997; Walsh & Watson 2005).

(*b*) *Hybrid lead sulphide composites*

Crystal structures for one-dimensional and three-dimensional hybrid organic–inorganic PbS composite networks have recently been determined (Turner *et al.* 2008), which are illustrated in figure 1. The experimental structural parameters, measured at room temperature using powder X-ray diffraction, were taken as the starting positions, which were then fully relaxed through DFT calculations, with the resulting equilibrium structures and band gaps detailed in table 1.

The crystal structure of the three-dimensional hybrid system, $Pb_3(C_6S_6)$, is hexagonal (space group 191, P6/mmm) with one formula unit per repeating cell. The structure consists of alternating planes of Pb and S/C oriented along of the c-axis. Each Pb atom lies at the centre of a cube with eightfold sulphur coordination, while each S atom is coordinated to four lead atoms and one carbon atom. The carbon atoms form sulphur-terminated planar hexagonal rings, i.e. a derivative of benzenehexathiol. The equilibrium GGA structural parameters are in good agreement with experiment, with errors of less than 1.5 per cent.

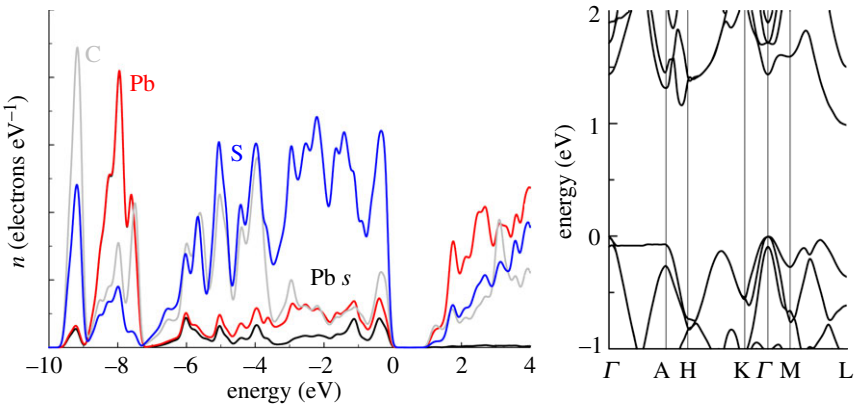

Figure 4. The local electronic density of states and band structure of the three-dimensional PbS hybrid material at the GGA level of theory. The highest occupied state is set to 0 eV. (Online version in colour.)

The electronic density of states of the hybrid system contains significant differences in comparison to bulk PbS, as shown in figure 4. The sulphur states in the valence band become more broadened due to the addition of interactions between C and S. Of particular note are the new localized peaks found at *ca.* −9.5 eV (π bonding between C and S) and at the top of the valence band (π^* antibonding). The Pb states remain largely unchanged, with the presence of the Pb 6*s* derived peak below −8 eV, and additional contributions at the top of the valence band.

Unlike the PbS host itself, the fundamental band gap of $Pb_3(C_6S_6)$ becomes indirect between the gamma point (valence band) and the L point (conduction band). This occurrence can be rationalized by exploring the band and *k*-point decomposed electron density arising from the band-edge states, with the corresponding density isosurfaces plotted in figure 5. For rocksalt structured PbS, coupling between Pb 6*s* and S 3*p* is symmetry forbidden at the gamma point, but occurs at the L point, which becomes the valence band maximum. In the hybrid material, the addition of the benzenehexathiol derivative raises the valence band energy further and it is instead the filled antibonding (π^*) states, arising from the interaction between the aromatic ring and the S 3*p* orbitals, which dominate at the top of the valence band. While the electron density arising from the gamma and L points appears similar, additional coupling with Pb 6*s* at the L point stabilizes the antibonding interactions, which lowers the band, making the valence band maximum occur at the gamma point. Conversely, the lowest lying conduction band at the gamma point is dominated by overlap between Pb 6*p* orbitals, while at the L point the Pb 6*p* interactions are out of phase and substantial contributions are present from π^* interactions within the S-C network. Optical transitions across the fundamental band gap will therefore involve excitations with significant contributions from the aromatic framework. This is in contrast to what has recently been reported for a hybrid titania framework, where the conduction band remains dominated by the inorganic network (Ti 3*d* orbitals) (Walsh & Catlow 2010).

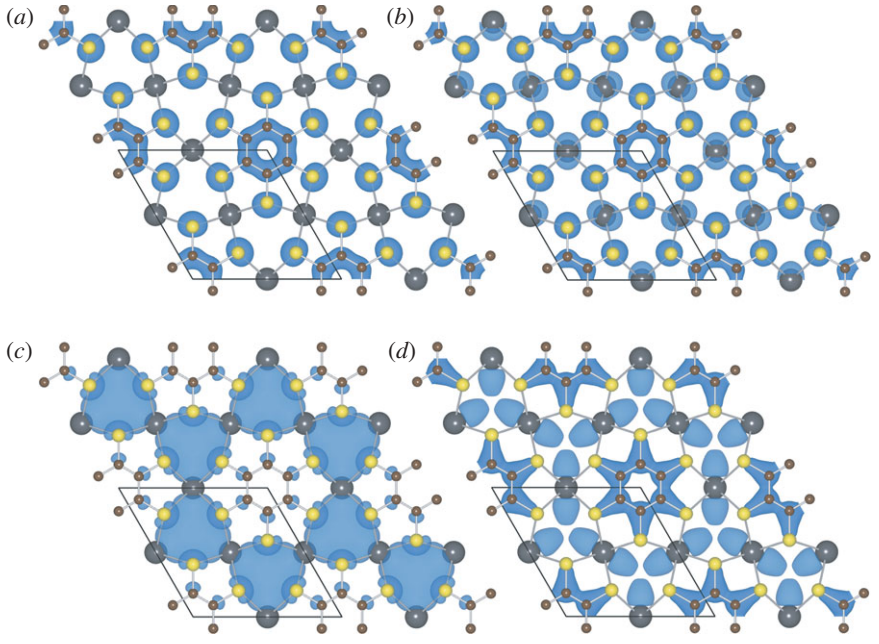

Figure 5. Electron density arising from the highest occupied band at the (*a*) Γ and (*b*) L points and the lowest unoccupied bands at the (*c*) Γ and (*d*) L points for the three-dimensional hybrid material. The carbon atoms are coloured brown, with grey Pb, yellow S and pink hydrogen. (Online version in colour.)

Now, we turn to the quasi-one-dimensional hybrid PbS system, $Pb_2(S_4C_6H_2)$ (*en*), which adopts a low symmetry triclinic structure (space group 2,$P\bar{1}$), with Pb and S occupying the Wyckoff 2*i* positions. There are two formula units present per repeating cell. In addition to the benzenethiol derivates (here benzene-1,2,4,5-tetrathiol), which were present in the three-dimensional hybrid networks, this system also contains a bidentate ethylenediamine ligand, with each of the terminating NH_2 groups chelated to a single Pb atom. The four remaining Pb–S bonds are present on one side of the Pb atom, similar to the Pb coordination environment in litharge PbO. The PbS polyhedra form one-dimensional chains along of the [100] direction, with the aromatic networks stacked along (201) planes.

The calculated local electronic density of states is shown in figure 6 for each of the sub units composing the hybrid network: the PbS polyhedra, the benzenehexathiol groups and the *en* ligands. Note that the same S atoms are shared between the organic and inorganic sub-networks. The low crystal symmetry results in more localized features in comparison to the previous systems; however, the main characteristics of the parent PbS compound remain present: the Pb 6*s* derived peak at −8 eV and the dominance of S 3*p* at the top of the valence band.

The effect of quantum confinement can be observed on the calculated electronic band gap, which is significantly larger (2.22 eV) in comparison to bulk PbS (0.47 eV) and the three-dimensional PbS network (0.99 eV); bulk PbS has a large

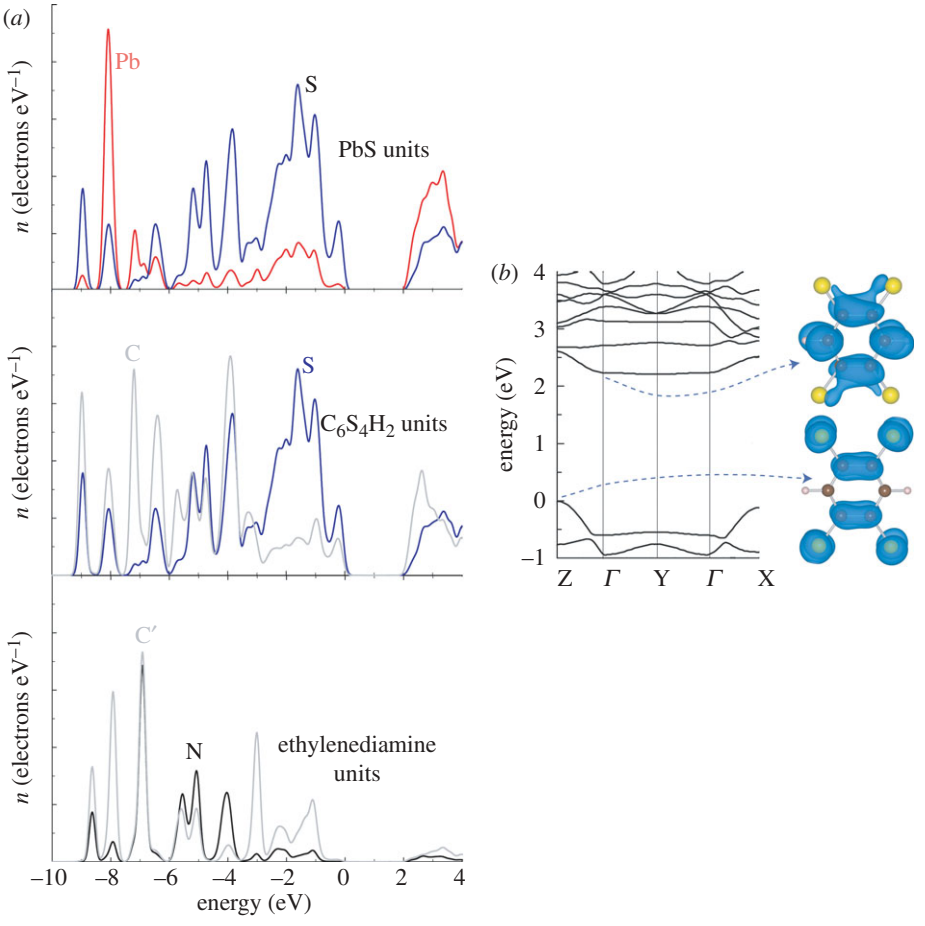

Figure 6. (*a*) Local electronic density of states for each component of the one-dimensional hybrid PbS material, $Pb_2(S_4C_6H_2)(en)$; the highest occupied state is set to zero. (*b*) Electronic band structure and band-edge electron density of $Pb_2(S_4C_6H_2)(en)$. (Online version in colour.)

Bohr excition radius of 20 nm, which gives the material a high susceptibility to strong-confinement effects (Wise 2000). Assessment of the band gaps using the hybrid HSE06 functional provides an upper limit, as it overestimates the band gap of PbS itself (table 1). With both semi-local and non-local functionals, the same trend is maintained: the band gap of bulk PbS is increased as the dimensionality of the inorganic network is reduced; it is worth noting that similar band gaps to the hybrid materials can be found for PbS quantum dots with radii between 4 and 8 nm.

Other key additions to the electronic density of states are the wide distribution of carbon states arising from the presence of two inequivalent carbon atoms in the aromatic network and the addition of the sp^3 hybridized carbons in the ethylenediamine ligand. The band structure confirms that this material has an indirect band gap, with both band-edge states arising from orbitals localized on the aromatic sub-network, as shown in figure 6.

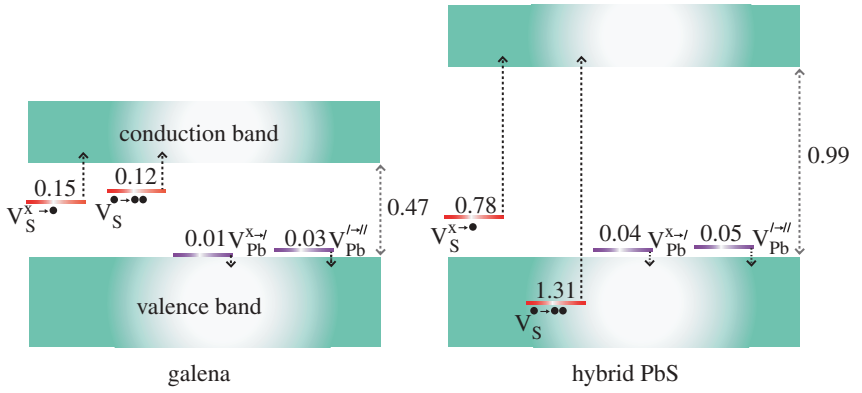

Figure 7. Schematic of the adiabatic defect ionization levels within the band gap of the bulk and hybrid PbS systems calculated using density functional theory at the GGA level. (Online version in colour.)

Table 2. Point defect reaction energies.

defect reaction	bulk PbS	three-dimensional hybrid
$S_S \rightleftharpoons V_S^{\times} + S(s)$	1.77	2.47
$Pb_{Pb} \rightleftharpoons V_{Pb}^{\times} + Pb(s)$	1.36	1.74
$Pb_{Pb} + S_S \rightleftharpoons V_{Pb}^{\times} + V_S^{\times} + PbS(s)$	1.04	1.58
$Pb_{Pb} + S_S \rightleftharpoons V_{Pb}^{/} + V_S^{\bullet} + PbS(s)$	0.87	1.43
$Pb_{Pb} + S_S \rightleftharpoons V_{Pb}^{//} + V_S^{\bullet\bullet} + PbS(s)$	0.69	1.55

For the hybrid material, the Schottky reaction is balanced through the precipitation of bulk PbS. All values are in eV per defect.

(*c*) *Defect chemistry*

Analysis of the intrinsic defect reactions in the bulk and three-dimensional hybrid PbS systems, the details of which have been presented elsewhere (Walsh 2010), have indicated a particularly low formation energy and shallow ionization levels for cation vacancies, which would suggest that the hybrid materials will favour intrinsic *p*-type behaviour. The defect reaction energies are listed in table 2, with the thermal ionization levels shown in figure 7. As the top of the valence band is composed of antibonding interactions between S 3*p* and Pb 6*s* in PbS (Walsh & Watson 2005), emptying these states is accompanied by only a small energetic penalty, similar to the antibonding O 2*p*/Cu 3*d* states in the *p*-type oxide semiconductor Cu_2O (Nolan & Elliott 2006; Scanlon *et al.* 2009; Soon *et al.* 2009). The same orbital character is observed in the high-energy bands of the three-dimensional hybrid material with the addition of delocalized π^* states.

In contrast to the lead vacancy, the sulphur vacancy in PbS results in a deep defect level, predominately localized in the vacancy site, i.e. an F-centre (or colour centre), which may be viewed as a two-electron He analogous to the hydrogenic one-electron F-centre observed in alkali halides (Stoneham 1975). In this case,

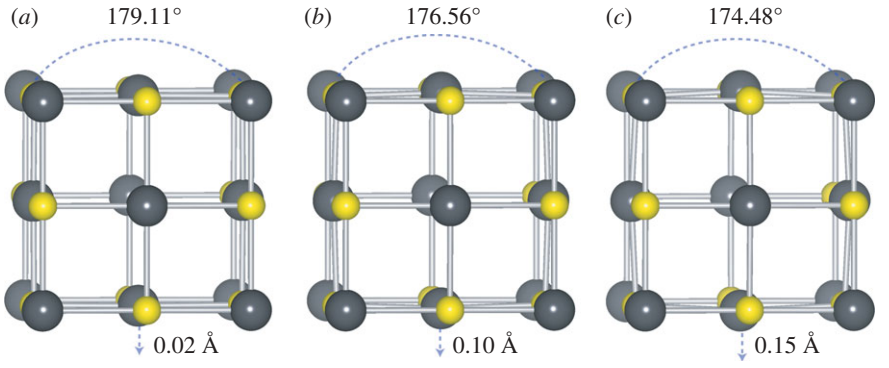

Figure 8. Equilibrium geometries around (*a*) $V_S^{\times}$, (*b*) $V_S^{\bullet}$ and (*c*) $V_S^{\bullet\bullet}$ in galena. The S–Pb–S bond angles and Pb displacements, shown relative to the ideal bulk positions, are isotropic around the defect site. (Online version in colour.)

the F-centre is accompanied by significant polarization of the neighbouring Pb sites. In the hybrid material, the defect charge density is again associated with a localized centre, but there is additional hybridization with the neighbouring π framework: see Walsh (2010).

Ionization of the localized anion vacancy centres shows different behaviour in the bulk and hybrid systems: the F^+ centre is thermodynamically unstable in PbS, exhibiting negative U behaviour, where U represents the on-site repulsive Coulomb interaction between two electrons (Anderson 1975; Yu & Cardona 2005). In such a case, negative U refers to the situation where the second electron is *attracted* to the defect state, and a direct transition is observed between the closed shell neutral and doubly ionized point defect centres. In other words, in thermal equilibrium, the F^+ centre will only be metastable: for any equilibrium position of the Fermi energy within the band gap, the defect state will exist either as an F or F^{++} centre. Ionization of $V_S^{\times}$ in galena results in an isotropic outward expansion of the neighbouring Pb ions as shown in figure 8. In the hybrid material, similar ionic relaxation occurs but the $V_S^{\bullet}$ centre is further stabilized electronically due to interaction with the organic sub-lattice, and the $V_S^{\bullet\rightarrow\bullet\bullet}$ transition lies resonant within the valence band. If produced in sufficient quantities, the paramagnetic $V_S^{\bullet}$ centre should be observable through spectroscopic methods, such as electron spin resonance.

The energies for Schottky pair formation (intrinsic ionic disorder involving non-interacting site vacancies) are listed in table 2. Both materials exhibit a preference for charged Schottky formation owing to the beneficial electron transfer between donor and acceptor states; however, the charge state preferences differ in the two cases: PbS favours doubly charged (fully ionized) disorder, while $Pb_3(C_6S_6)$ favours the single ionized Schottky disorder as the defect level of $V_S^{\bullet\bullet}$ lies *below* that of $V_{Pb}^{//}$. The Schottky energies, ranging from 0.7 to 1.6 eV per defect, are much smaller than those observed in wide band gap metal oxide and III–V systems, e.g. 4.44 eV in In_2O_3 (Walsh *et al.* 2009*a*), 3.45 eV in ZnO (Sokol *et al.* 2007; Catlow *et al.* 2008), 3.67 eV in SnO_2 (Godinho *et al.* 2009), and 4.7 eV in GaN (Catlow *et al.* 2010). For all defect reactions, the formation energies

are substantially higher in the hybrid materials, which would suggest that their concentrations will be much lower: to produce semiconducting samples, it may be necessary to extrinsically dope these materials.

4. Discussion

A number of key changes have been observed in the transition from bulk PbS to the quasi-one-dimensional hybrid PbS material. Bulk PbS is a direct band gap, low effective mass semiconductor. On transition to the three-dimensional hybrid network, the local PbS bonding network is perturbed and the valence and conduction band-edge states contain contributions from hybridized states of both the organic and inorganic sub-networks. However, while the band gap is opened, significant band dispersion is maintained, which should contribute to reasonable carrier mobility in the hybrid materials. Unfortunately, indirect band gaps are predicted, which could limit radiative recombination of electrons and holes for light-emission applications. Investigation of the primary defect reactions suggests that a number of parallels exist between the bulk and hybrid systems; most importantly, Pb vacancies exist as low energy shallow electron accepting defects in both cases, while sulphur vacancies exist as deep colour centres. In all materials studied, the contribution of the organic ligands to the band-edge states is appreciable, and the resulting electron transport properties will therefore rely on the cooperative behaviour between the inorganic and organic networks.

Three avenues for chemical functionalization can be envisioned in hybrid materials, which extend beyond the prototype PbS compounds studied here:

— In terms of the aromatic ligands, incorporation of acidic or basic functional groups could be used to engineer the band-edge positions (adjusting the effective ionization potentials and electron affinities), which in turn will affect both the visible light absorption and defect properties. Direct examples would include the substitution of electron withdrawing groups such as an alcohol, amine or triflouromethyl compounds into the aromatic ring, or the addition of electron donating groups such as a methyl or aldehyde derivative.
— In terms of the inorganic network, similar frameworks could be built, while maintaining the underlying II–VI framework, for example, the replacement of Pb with alternative divalent cationic species such as Sn, Cd or Zn. Partial substitutions to form hybrid II–VI alloys, e.g. (Zn,Sn)S materials, may also be feasible considering the mechanical flexibility of the organic network to compensate for alloy strain. Alternatively, cation mutation could be performed producing multi-ternary semiconductors analogous to chalcopyrite (e.g. $CuGaSe_2$) and kesterite (e.g. $CuZnSnS_4$) solar cell absorbers (Goodman 1958; Chen *et al.* 2009*a*,*b*, 2010).
— Isoelectronic modification of the anions is also feasible, forming the corresponding oxides, selenides or tellurides. In most cases, oxide formation would be expected to increase the band gap, through the addition of more localized, higher binding energy, O 2*p* orbitals and enhanced electron transfer. Conversely, the addition of Te would be expected to decrease the band gap. Forming intermediate systems of

mixed composition, e.g. oxysulphide hybrid compounds, would introduce an extra degree of freedom, as demonstrated by the purely inorganic oxysulphide class of *p*-type transparent oxide semiconductors (Ueda *et al.* 2000; Scanlon & Watson 2009).

A computational exploration of these design principles is currently in progress.

5. Conclusions

Using first-principles electronic structure calculations, we have investigated the changes in electronic structure and chemical bonding on transition from bulk PbS to hybrid organic–inorganic networks containing three and one dimensionalities in the PbS interactions. In particular, our analysis highlighted:

— The contributions of the aromatic subnetworks to the band-edge states active in electron transport.
— A large *increase* in electronic band gap on formation of the hybrid compounds comparable to PbS quantum dots with radii of 4 to 8 nm.
— Comparable defect chemistry between the hybrid and inorganic parent PbS systems.
— Accessible routes for chemical engineering of the electronic properties of hybrid materials.

The results emphasize the potential of hybrid materials as functional semiconducting materials, an area that is presently growing, and can result in viable new directions for obtaining materials chemically engineered for photovoltaic and optoelectronic devices. The role of materials simulation in providing predictive guidance can help to rapidly progress research in this area.

I would like to acknowledge stimulating discussions with T. P. Vaid, A. K. Cheetham, C. R. A. Catlow, A. A. Sokol, S. M. Woodley and D. Demathieu. This work was funded through a Marie-Curie Intra-European Fellowship on 'Electronic Structure Modelling of Hybrid Organic-Inorganic Semiconductors' from the European Union under the Seventh Framework Programme. Via my membership of the UK's HPC Materials Chemistry Consortium, which is funded by EPSRC (EP/F067496), this work made use of the facilities of HECToR, the UK's national high-performance computing service. I also acknowledge use of the UCL Legion High Performance Computing Facility, and associated support services, in the completion of this work.

References

Alvaro, M., Carbonell, E., Belén, F., Llabrés, I., Xamena, F. X. & Hermenegildo, G. 2007 Semiconductor behavior of a metal–organic framework (MOF). *Chem. Eur. J.* **13**, 5106–5112. (doi:10.1002/chem.200601003)

Anderson, P. W. 1975 Model for the electronic structure of amorphous semiconductors. *Phys. Rev. Lett.* **34**, 953–955. (doi:10.1103/PhysRevLett.34.953)

Aroyo, M. I., Kirov, A., Capillas, C., Perez-Mato, J. M. & Wondratschek, H. 2006 Bilbao crystallographic server. II. Representations of crystallographic point groups and space groups. *Acta Crystallogr. Sect. A* **62**, 115–128. (doi:10.1107/S0108767305040286)

Blöchl, P. E. 1994 Projector augmented-wave method. *Phys. Rev. B* **50**, 17 953–17 979. (doi:10.1103/PhysRevB.50.17953)

Brothers, E. N., Izmaylov, A. F., Normand, J. O., Barone, V. & Scuseria, G. E. 2008 Accurate solid-state band gaps via screened hybrid electronic structure calculations. *J. Chem. Phys.* **129**, 011102. (doi:10.1063/1.2955460)

Catlow, C. R. A., French, S. A., Sokol, A. A., Al-Sunaidi, A. A. & Woodley, S. M. 2008 Zinc oxide: a case study in contemporary computational solid state chemistry. *J. Comput. Chem.* **29**, 2234–2249. (doi:10.1002/jcc.21051)

Catlow, C. R. A., Guo, Z. X., Miskufova, M., Shevlin, S. A., Smith, A. G. H., Sokol, A. A., Walsh, A., Wilson, D. J. & Woodley, S. M. 2010 Advances in computational studies of energy materials. *Phil. Trans. R. Soc. A* **368**, 3379–3456. (doi:10.1098/rsta.2010.0111)

Cheetham, A. K. & Rao, C. N. R. 2007 Materials science: there's room in the middle. *Science* **318**, 58–59. (doi:10.1126/science.1147231)

Cheetham, A. K., Rao, C. N. R. & Feller, R. K. 2006 Structural diversity and chemical trends in hybrid inorganic–organic framework materials. *Chem. Comm.* **46**, 4780–4795. (doi:10.1039/b610264f)

Chen, S., Gong, X. G., Walsh, A. & Wei, S.-H. 2009*a* Crystal and electronic band structure of Cu_2ZnSnX_4 (X = S and Se) photovoltaic absorbers: first-principles insights. *Appl. Phys. Lett.* **94**, 041903. (doi:10.1063/1.3074499)

Chen, S., Gong, X. G., Walsh, A. & Wei, S.-H. 2009*b* Electronic structure and stability of quaternary chalcogenide semiconductors derived from cation cross-substitution of II–VI and I–III–VI_2 compounds. *Phys. Rev. B* **79**, 165211. (doi:10.1103/PhysRevB.79.165211)

Chen, S., Gong, X. G., Walsh, A. & Wei, S.-H. 2010 Defect physics of the kesterite thin-film solar cell absorber Cu_2ZnSnS_4. *Appl. Phys. Lett.* **96**, 021902. (doi:10.1063/1.3275796)

Corà, F., Alfredsson, M., Mallia, G., Middlemiss, D. S., Mackrodt, W. C., Dovesi, R. & Orlando, R. 2004 The performance of hybrid density functionals in solid state chemistry. *Chem. Mater. Sci.* **113**, 171–232. (doi:10.1007/b97944)

Dovesi, R., Causà, M. & Angonoa, G. 1981 Exact-exchange Hartree–Fock calculations for periodic systems. V. Ground-state properties of silicon. *Phys. Rev. B* **24**, 4177–4183. (doi:10.1103/PhysRevB.24.4177)

Ellingson, R. J., Beard, M. C., Johnson, J. C., Yu, P., Micic, O. I., Nozik, A. J., Shabaev, A. & Efros, A. L. 2005 Highly efficient multiple exciton generation in colloidal PbSe and PbS quantum dots. *Nano Lett.* **5**, 865–871. (doi:10.1021/nl0502672)

Ferey, G. 2001 Microporous solids: from organically templated inorganic skeletons to hybrid frameworks—ecumenism in chemistry. *Chem. Mater.* **13**, 3084–3098. (doi:10.1021/cm011070n)

Godinho, K. G., Walsh, A. & Watson, G. W. 2009 Energetic and electronic structure analysis of intrinsic defects in SnO_2. *J. Phys. Chem. C* **113**, 439–448. (doi:10.1021/jp807753t)

Goodman, C. H. L. 1958 The prediction of semiconducting properties in inorganic compounds. *J. Phys. Chem. Solids* **6**, 305–314. (doi:10.1016/0022-3697(58)90050-7)

Guo, Z., Cao, R., Wang, X., Li, H., Yuan, W., Wang, G., Wu, H. & Li, J. 2009 A Multifunctional 3D ferroelectric and NLO-active porous metal-organic framework. *J. Am. Chem. Soc.* **131**, 6894–6895. (doi:10.1021/ja9000129)

Heyd, J. & Scuseria, G. E. 2004 Efficient hybrid density functional calculations in solids: assessment of the Heyd–Scuseria–Ernzerhof screened Coulomb hybrid functional. *J. Chem. Phys.* **121**, 1187–1192. (doi:10.1063/1.1760074)

Hohenberg, P. & Kohn, W. 1964 Inhomogeneous electron gas. *Phys. Rev.* **136**, B864–B871. (doi:10.1103/PhysRev.136.B864)

Huang, X., Roushan, M., Emge, T. J., Bi, W., Thiagarajan, S., Cheng, J.-H., Yang, R. & Li, J. 2009 Flexible hybrid semiconductors with low thermal conductivity: the role of organic diamines. *Angew. Chem. Int. Ed.* **48**, 7871–7874. (doi:10.1002/anie.200903234)

Hummer, K., Harl, J. & Kresse, G. 2009 Heyd–Scuseria–Ernzerhof hybrid functional for calculating the lattice dynamics of semiconductors. *Phys. Rev. B* **80**, 115205. (doi:10.1103/PhysRevB.80.115205)

Kohn, W. & Sham, L. J. 1965 Self-consistent equations including exchange and correlation effects. *Phys. Rev.* **140**, A1133–A1138. (doi:10.1103/PhysRev.140.A1133)

Kresse, G. & Furthmüller, J. 1996*a* Efficiency of *ab initio* total energy calculations for metals and semiconductors using a plane-wave basis set. *Comput. Mater. Sci.* **6**, 15–50. (doi:10.1016/0927-0256(96)00008-0)

Kresse, G. & Furthmüller, J. 1996*b* Efficient iterative schemes for *ab initio* total-energy calculations using a plane-wave basis set. *Phys. Rev. B* **54**, 11 169–11 186. (doi:10.1103/PhysRevB.54.11169)

Lin, H. & Maggard, P. A. 2007 Copper(I)-rhenate hybrids: syntheses, structures, and optical properties. *Inorg. Chem.* **46**, 1283. (doi:10.1021/ic061767g)

Lin, H. S. & Maggard, P. A. 2008 Synthesis and structures of a new series of silver–vanadate hybrid solids and their optical and photocatalytic properties. *Inorg. Chem.* **47**, 8044–8052. (doi:10.1021/ic8004129)

Lin, H. S., Wu, X. M. & Maggard, P. A. 2009 Ligand-based modification of the structures and optical properties of new silver(i)-rhenate(vii) oxide/organic hybrid solids. *Inorg. Chem.* **48**, 11 265–11 276. (doi:10.1021/ic901749r)

Madelung, O. M. 2004 *Semiconductors: data handbook*. Berlin, Germany: Springer.

Marsman, M., Paier, J., Stroppa, A. & Kresse, G. 2008 Hybrid functionals applied to extended systems. *J. Phys. Condensed Matter* **20**, 064201. (doi:10.1088/0953-8984/20/6/064201)

McGuinness, C., Stagarescu, C. B., Ryan, P. J., Downes, J. E., Fu, D., Smith, K. E. & Egdell, R. G. 2003 Influence of shallow core-level hybridization on the electronic structure of post-transition-metal oxides studied using soft X-ray emission and absorption. *Phys. Rev. B* **68**, 165104. (doi:10.1103/PhysRevB.68.165104)

Mellot-Draznieks, C. 2007 Role of computer simulations in structure prediction and structure determination: from molecular compounds to hybrid frameworks. *J. Mater. Chem.* **17**, 4348–4358. (doi:10.1039/b702516p)

Murnaghan, F. D. 1944 The compressibility of media under extreme pressures. *Proc. Natl Acad. Sci. USA* **30**, 244–247. (doi:10.1073/pnas.30.9.244)

Nolan, M. & Elliott, S. D. 2006 The p-type conduction mechanism in Cu_2O: a first principles study. *Phys. Chem. Chem. Phys.* **8**, 5350–5358. (doi:10.1039/b611969g)

Nozik, A. J. 2005 Exciton multiplication and relaxation dynamics in quantum dots: applications to ultrahigh-efficiency solar photon conversion. *Inorg. Chem.* **44**, 6893–6899. (doi:10.1021/ic0508425)

Paier, J., Marsman, M., Hummer, K., Kresse, G., Gerber, I. C. & Angyan, J. G. 2006 Screened hybrid density functionals applied to solids. *J. Chem. Phys.* **124**, 154709. (doi:10.1063/1.2187006)

Payne, D. J., Egdell, R. G., Walsh, A., Watson, G. W., Guo, J., Glans, P. A., Learmonth, T. & Smith, K. E. 2006 Electronic origins of structural distortions in post-transition metal oxides: experimental and theoretical evidence for a revision of the lone pair model. *Phys. Rev. Lett.* **96**, 157403. (doi:10.1103/PhysRevLett.96.157403)

Perdew, J. P., Burke, K. & Ernzerhof, M. 1996 Generalized gradient approximation made simple. *Phys. Rev. Lett.* **77**, 3865–3868. (doi:10.1103/PhysRevLett.77.3865)

Rao, C. N. R., Cheetham, A. K. & Thirumurugan, A. 2008 Hybrid inorganic–organic materials: a new family in condensed matter physics. *J. Phys.: Condensed Matter* **20**, 083202. (doi:10.1088/0953-8984/20/8/083202)

Scanlon, D. O. & Watson, G. W. 2009 $(Cu_2S_2)(Sr_3Sc_2O_5)$–a layered, direct band gap, p-type transparent conducting oxychalcogenide: a theoretical analysis. *Chem. Mater.* **21**, 5435–5442. (doi:10.1021/cm902260b)

Scanlon, D. O., Morgan, B. J., Watson, G. W. & Walsh, A. 2009 Acceptor levels in p-type Cu_2O: rationalizing theory and experiment. *Phys. Rev. Lett.* **103**, 096405. (doi:10.1103/PhysRevLett.103.096405)

Shockley, W. & Queisser, H. J. 1961 Detailed balance limit of efficiency of p–n junction solar cells. *J. Appl. Phys.* **32**, 510. (doi:10.1063/1.1736034)

Sokol, A. A., French, S. A., Bromley, S. T., Catlow, C. R. A., Dam, H. J. J. V. & Sherwood, P. 2007 Point defects in ZnO. *Faraday Discussions* **134**, 267–282. (doi:10.1039/b607406e)

Soon, A., Cui, X.-Y., Delley, B., Wei, S.-H. & Stampfl, C. 2009 Native defect-induced multifarious magnetism in nonstoichiometric cuprous oxide: first-principles study of bulk and surface properties of Cu_2O. *Phys. Rev. B* **79**, 035205. (doi:10.1103/PhysRevB.79.035205)

Srivastava, G. P., Martins, J. L. & Zunger, A. 1985 Atomic structure and ordering in semiconductor alloys. *Phys. Rev. B* **31**, 2561–2564. (doi:10.1103/PhysRevB.31.2561)

Stoneham, A. M. 1975 *Theory of defects in solids*. New York, NY: Oxford University Press.

Turner, D. L., Vaid, T. P., Stephens, P. W., Stone, K. H., Dipasquale, A. G. & Rheingold, A. L. 2008 Semiconducting lead–sulfur-organic network solids. *J. Am. Chem. Soc.* **130**, 14–15. (doi:10.1021/ja0770983)

Ueda, K., Inoue, S., Hirose, S., Kawazoe, H. & Hosono, H. 2000 Transparent p-type semiconductor: LaCuOS layered oxysulfide. *Appl. Phys. Lett.* **77**, 2701–2703. (doi:10.1063/1.1319507)

Walsh, A. 2010 Defect processes in a PbS metal organic framework: a quantum-confined hybrid semiconductor. *J. Phys. Chem. Lett.* **1**, 1284–1287. (doi:10.1021/jz100312y)

Walsh, A. & Catlow, C. R. A. 2010 Photostimulated reduction processes in a titania hybrid metal–organic framework. *Chem. Phys. Chem.* **11**, 2341–2344. (doi:10.1002/cphc.201000306)

Walsh, A. & Watson, G. W. 2004 Electronic structures of rocksalt, litharge, and herzenbergite SnO by density functional theory. *Phys. Rev. B* **70**, 235114. (doi:10.1103/PhysRevB.70.235114)

Walsh, A. & Watson, G. W. 2005 The origin of the stereochemically active Pb(II) lone pair: DFT calculations on PbO and PbS. *J. Solid State Chem.* **178**, 1422–1428. (doi:10.1016/j.jssc.2005.01.030)

Walsh, A., Da Silva, J. L. F. & Wei, S.-H. 2008 Theoretical description of magnetism in cobalt doped ZnO. *Phys. Rev. Lett.* **100**, 256401.

Walsh, A., Catlow, C. R. A., Sokol, A. A. & Woodley, S. M. 2009*a* Physical properties, Intrinsic defects, and phase stability of indium sesquioxide. *Chem. Mater.* **21**, 4962–4969. (doi:10.1021/cm902280z)

Walsh, A., Da Silva, J. L. F., Yan, Y., Al-Jassim, M. M. & Wei, S.-H. 2009*b* Origin of electronic and optical trends in ternary $In_2O_3(ZnO)_n$ transparent conducting oxides ($n = 1,3,5$): Hybrid density functional theory calculations. *Phys. Rev. B* **79**, 073105. (doi:10.1103/PhysRevB.79.073105)

Walsh, A., Yan, Y., Huda, M. N., Al-Jassim, M. M. & Wei, S.-H. 2009*c* Band edge electronic structure of $BiVO_4$: elucidating the role of the Bi s and V d orbitals. *Chem. Mater.* **21**, 547–551. (doi:10.1021/cm802894z)

Wei, S.-H. & Zunger, A. 1997 Electronic and structural anomalies in lead chalcogenides. *Phys. Rev. B* **55**, 13605. (doi:10.1103/PhysRevB.55.13605)

Wei, S.-H., Ferreira, L. G., Bernard, J. E. & Zunger, A. 1990 Electronic properties of random alloys: special quasirandom structures. *Phys. Rev. B* **42**, 9622–9649. (doi:10.1103/PhysRevB.42.9622)

Wise, F. W. 2000 Lead salt quantum dots: the limit of strong quantum confinement. *Accounts Chem. Res.* **33**, 773–780. (doi:10.1021/ar970220q)

Wright, K., Hillier, I. H., Vaughan, D. J. & Vincent, M. A. 1999*a* Cluster models of the dissociation of water on the surface of galena (PbS). *Chem. Phys. Lett.* **299**, 527–531. (doi:10.1016/S0009-2614(98)01312-8)

Wright, K., Hillier, I. H., Vincent, M. A. & Kresse, G. 1999*b* Dissociation of water on the surface of galena (PbS): a comparison of periodic and cluster models. *J. Chem. Phys.* **111**, 6942–6946. (doi:10.1063/1.479986)

Yu, P. Y. & Cardona, M. 2005 *Fundamentals of semiconductors*. Berlin, Germany: Springer.

Zemel, J. N., Jensen, J. D. & Schoolar, R. B. 1965 Electrical and optical properties of epitaxial films of PbS, PbSe, PbTe, and SnTe. *Phys. Rev.* **140**, A330–A342. (doi:10.1103/PhysRev.140.A330)

Zhang, Y., Dalpian, G. M., Fluegel, B., Wei, S.-H., Mascarenhas, A., Huang, X. Y., Li, J. & Wang, L. W. 2006 Novel approach to tuning the physical properties of organic–inorganic hybrid semiconductors. *Phys. Rev. Lett.* **96**, 026405. (doi:10.1103/PhysRevLett.96.026405)

Zhu, Y. Z., Chen, G. D., Ye, H. G., Walsh, A., Moon, C. Y. & Wei, S.-H. 2008 Electronic structure and phase stability of MgO, ZnO, CdO, and related ternary alloys. *Phys. Rev. B* **77**, 245209. (doi:10.1103/PhysRevB.77.245209)